

Analysis of contact stiffness in ultrasound atomic force microscopy: three-dimensional time-dependent ultrasound modeling

This content has been downloaded from IOPscience. Please scroll down to see the full text.

2017 J. Phys. D: Appl. Phys. 50 235601

(<http://iopscience.iop.org/0022-3727/50/23/235601>)

View [the table of contents for this issue](#), or go to the [journal homepage](#) for more

Download details:

IP Address: 139.63.41.237

This content was downloaded on 17/05/2017 at 08:40

Please note that [terms and conditions apply](#).

You may also be interested in:

[Visualization of subsurface nanoparticles in a polymer matrix using resonance tracking atomic force acoustic microscopy and contact resonance spectroscopy](#)

Kuniko Kimura, Kei Kobayashi, Atsushi Yao et al.

[Study of mechanical behavior of AFM silicon tips under mechanical load](#)

M Kopycinska-Mueller, J Gluch and B Köhler

[Characterization of piezoelectric ceramics](#)

U Rabe, M Kopycinska, S Hirsekorn et al.

[Micromechanical Contact Stiffness Devices and Application for Calibrating Contact Resonance Atomic Force Microscopy](#)

Matthew R Rosenberger, Sihan Chen, Craig B Prater et al.

[Subsurface imaging of two-dimensional materials on the nanoscale](#)

Franco Dinelli, Pasqualantonio Pingue, Nicholas D Kay et al.

[Intermittent contact resonance atomic force microscopy](#)

Gheorghe Stan and Richard S Gates

[Nanoscale tomographic reconstruction of the subsurface mechanical properties of low-k high-aspect ratio patterns](#)

Gheorghe Stan, Ebony Mays, Hui Jae Yoo et al.

[Subsurface contrast due to friction in Heterodyne Force Microscopy](#)

G J Verbiest, T H Oosterkamp and M J Rost

Analysis of contact stiffness in ultrasound atomic force microscopy: three-dimensional time-dependent ultrasound modeling

Daniele Piras and Hamed Sadeghian

Netherlands Organization for Applied Scientific Research, TNO, 2628 CK Delft, The Netherlands

E-mail: hamed.sadeghianmarnani@tno.nl

Received 27 January 2017, revised 3 April 2017

Accepted for publication 28 April 2017

Published 16 May 2017




Abstract

Ultrasound atomic force microscopy (US-AFM) has been used for subsurface imaging of nanostructures. The contact stiffness variations have been suggested as the origin of the image contrast. Therefore, to analyze the image contrast, the local changes in the contact stiffness due to the presence of subsurface features should be calculated. So far, only static simulations have been conducted to analyze the local changes in the contact stiffness and, consequently, the contrast in US-AFM. Such a static approach does not fully represent the real US-AFM experiment, where an ultrasound wave is launched either into the sample or at the tip, which modulates the contact stiffness. This is a time-dependent nonlinear dynamic problem rather than a static and stationary one. This paper presents dynamic 3D ultrasound analysis of contact stiffness in US-AFM (in contrast to static analysis) to realistically predict the changes in contact stiffness and thus the changes in the subsurface image contrast. The modulation frequency also influences the contact stiffness variations and, thus, the image contrast. The three-dimensional time-dependent ultrasound analysis will greatly aid in the contrast optimization of subsurface nano imaging with US-AFM.

Keywords: contact stiffness, ultrasound AFM, nanoimaging, Hertz contact, subsurface AFM, subsurface nanoimaging

(Some figures may appear in colour only in the online journal)

Atomic force microscopy (AFM) was initially developed for topographic imaging [1–3]. In AFM, a vibrating cantilever with a sharp tip scans a sample surface, which in turn, influences the deflection of the same cantilever. The motion of the cantilever is measured with the use of the optical beam deflection method [4, 5] and gives a high resolution image of the surface [6]. In dynamic mode AFM, the tip–sample interaction influences the vibration mode of the cantilever [7]. The response of the cantilever specifically depends on the tip–sample interaction stiffness, i.e. the so-called contact stiffness. The local variations in contact stiffness change the contact resonance frequency of the cantilever and its vibration mode [8].

 Original content from this work may be used under the terms of the [Creative Commons Attribution 3.0 licence](https://creativecommons.org/licenses/by/3.0/). Any further distribution of this work must maintain attribution to the author(s) and the title of the work, journal citation and DOI.

The further combination with ultrasonic excitation resulted in a variety of methods like UFM [9], AFAM [10, 11], UAFM [7], HFM [12]. We simply refer to ultrasound-AFM (US-AFM) to indicate the common ultrasonic excitation of the different AFM schemes mentioned above. In US-AFM either the tip or the sample is excited with an ultrasonic wave. At ultrasound frequencies (tens of MHz), the cantilever is effectively stiffened, and its stiffness can be tuned to match the stiffness of the contact, improving the image contrast [8, 10, 13]. With US-AFM, the possibility of imaging objects below the surface of a sample has been shown [10–12, 14]. Such subsurface imaging capabilities are of great interest in several fields, such as semiconductors [15], life sciences [16], and measurements of local mechanical properties [17].

To analyze and enhance the image contrast in US-AFM or to extract quantitative material properties, the local changes

in contact stiffness should be determined [11, 18]. Static and stationary simulations have been performed [8] to predict the changes in the contact stiffness. However, static simulations do not fully represent the nonlinear dynamic situation of US-AFM since the effect of ultrasound waves on the contact stiffness is a time-dependent, dynamic problem. The dynamic behavior of the motion of the cantilever is influenced by the tip-sample interaction, specifically the contact stiffness, and exhibits a different resonance frequency when the tip is probing on top or far away from a subsurface feature [12]. This mechanism is responsible for the subsurface imaging contrast and can be evaluated by measuring the changes in contact resonance.

To accurately analyze the contact stiffness in US-AFM, we performed three-dimensional time-dependent ultrasound calculations using the finite element method (FEM), which better represents the actual experimental conditions. Before addressing the time-dependent ultrasound calculations, we first recall the basics of contact theory and describe the FEM simulations for the static stationary case. This later allows a comparison with the time-dependent ultrasound results.

An implementation of a three-dimensional tip-sample contact problem using FEM has been described in [18] to estimate the effect of a scanning tip on the contact stiffness in static condition primarily for cavity-like structures (voids). This approach has been reported to be extremely time consuming due to the required fine discretization at the contact area. We followed the same contact approach, and to reduce the computation time and the required memory, we also implemented a semi-analytical approach based on Hertzian contact theory [19, 20].

For a spherical tip (radius R) pressing with a constant force F on a semi-infinite and homogeneous medium in the absence of dissipative effects, the contact radius and the local stress distribution are respectively:

$$R_c = \sqrt[3]{2R\left(\frac{3}{8}\right)F(M_{\text{tip}} + M_{1\text{st layer}})} \quad (1)$$

$$P_c(x, y) = \frac{3F}{2\pi R_c^2} \sqrt{1 - \left(\frac{x^2 + y^2}{R_c^2}\right)}. \quad (2)$$

In equation (1)–(2), (x, y) are the coordinates of the points on the surface of the 1st layer (figure 1). The reduced Young's moduli of the tip and first layer are respectively:

$$M_{\text{tip}} = \frac{E_{\text{tip}}}{(1 - \nu_{\text{tip}}^2)} \quad (3)$$

$$M_{1\text{st layer}} = \frac{E_{1\text{st layer}}}{(1 - \nu_{1\text{st layer}}^2)} \quad (4)$$

where ν indicates Poisson's ratio, and E Young's modulus. In the semi-analytical FEM approach the analytical expression of stress distribution $P_c(x, y)$ is imposed as a distributed load on the contact area defined by R_c .

The output of the FEM analysis (both the contact and the semi-analytical implementation) is the indentation depth δ of

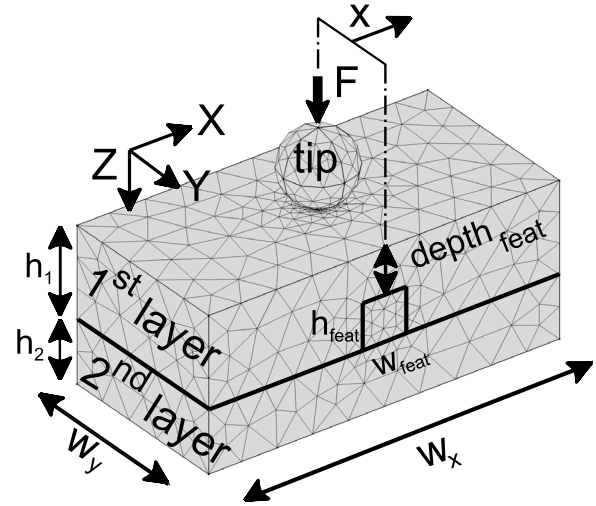


Figure 1. Schematic illustration of the geometry used for FEM calculation. The origin of the system of reference coincides with the tip-first layer contact point. The x -axis coincides with the feature (or inclusion) scan direction.

the tip into the sample. The indentation depends on the sample structure, on the embedded finite size feature and on its position relative to the tip. The indentation is used to make a new estimate [18, 21] of the reduced Young's modulus of the first layer:

$$\langle M_{1\text{st layer}} \rangle = \sqrt{\frac{(3F/2\delta)^3}{6FR}}. \quad (5)$$

Finally, the contact stiffness K can be calculated as:

$$K = \sqrt[3]{6FR\langle E^* \rangle^2} \quad (6)$$

where:

$$\frac{1}{\langle E^* \rangle} = \frac{1}{M_{\text{tip}}} + \frac{1}{\langle M_{1\text{st layer}} \rangle} \quad (7)$$

is the reciprocal of the combined Young's modulus.

Before implementing the ultrasound (time-dependent) wave excitation, the semi-analytical approach has been verified in the static stationary case. We show the verification for one case of a rigid inclusion in a rigid matrix (table 1, case 2, $\text{depth}_{\text{feat}} = 100 \text{ nm}$, force $0.5 \mu\text{N}$). The feature is moved from right below the contact in steps of 10 nm , and the contact stiffness (K) at the tip-sample contact location is extracted at each scan step. The distance x (direction X in figure 1) between the center of the feature and the center of the tip defines the scan position. In figure 2(a) where x equals zero, the feature is exactly below the tip. Where the feature is far from the tip (e.g. $x = 300 \text{ nm}$ in figure 2(a)) the contact stiffness is defined as baseline contact stiffness ($K = K_b$). In figure 2(a) the contact stiffness variation (ΔK) with respect to the baseline contact stiffness (K_b) is reported for each FEM analysis approach, i.e. $\Delta K = K(x) - K_b$, where $K(x)$ is the contact stiffness estimation at scan position x .

Figure 2(a) shows that there is very good agreement between the outlined semi-analytical procedure (calculated in COMSOL) and the 3D full contact model (calculated in both

Table 1. Geometry used in FEM simulations. Case 1 is representative of a rigid inclusion in a soft matrix, while case 2 is representative of a rigid inclusion in a rigid matrix. The size of the layers and of the inclusion in the Z and X directions (figure 1) are indicated by h and w respectively. The size of all layers and of the feature in Y direction (w_y in figure 1) is 400 nm.

Case	Part	Material	Radius (nm)	Height (nm)	Width (nm)	Depth _{feat} (nm)	Force F(μ N)
1	Tip	Si	10 ^a ; 80				0.2; 0.5
	1st layer	PMMA		$h_1 = 400$	$w_x = 800$	300	
	Feature	Al		$h_{feat} = 100$	$w_{feat} = 100$		
	2nd layer	Si		$h_2 = 135$	$w_x = 800$		
2	Tip	C	10; 80				0.2; 0.5
	1st layer	SiO ₂		$h_1 = 200$	$w_x = 800$	100	
				$h_1 = 300$	$w_x = 800$	200	
	Feature	Si		$h_{feat} = 100$	$w_{feat} = 100$		
	2nd layer	Si		$h_2 = 135$	$w_x = 800$		

^aFor 10 nm tip radius of case 1 the applied force is reduced to 0.1, 0.2 and 0.3 μ N.

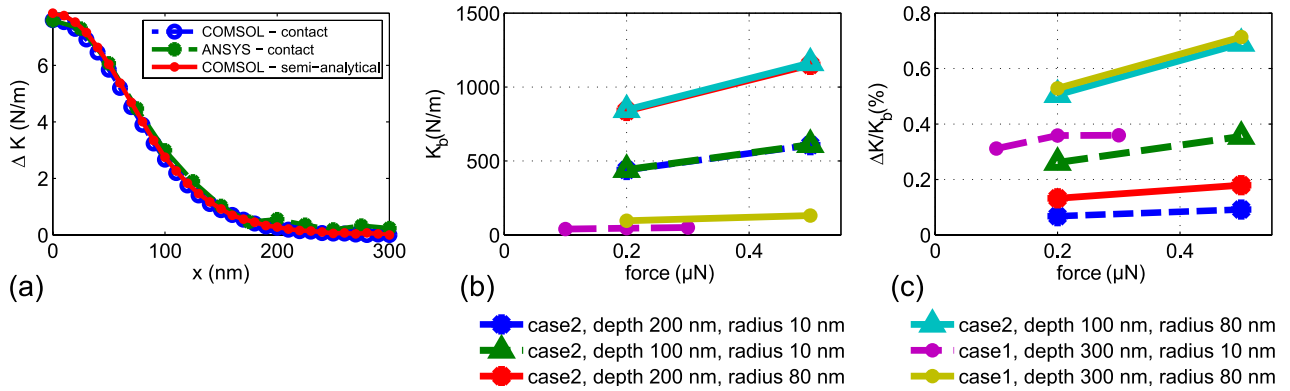


Figure 2. (a) Semi-analytical approach compared to the contact approach for the calculation of the static contact stiffness variation (table 1). For case 2, $depth_{feat}$ is 100 nm, and the applied force is 0.5 μ N. (b) Baseline contact stiffness ($K = K_b$) and (c) contact stiffness variation normalized to the baseline contact stiffness ($\Delta K/K_b$) for the use cases in table 1. In the legend, ‘depth’ indicates the depth of the inclusion ($depth_{feat}$), and ‘radius’ indicates the radius of the tip.

COMSOL and ANSYS). All three simulations show the same contact stiffness variation ΔK of about 7.5 N m^{-1} along the feature scan with a slight overestimation of the baseline contact stiffness for the semi-analytical procedure (1.8% and 1.7% with respect to the ANSYS contact model and COMSOL contact model, respectively) with the advantage of a substantial reduction in computation time from about 25 h to 25 min for a complete scan (on an Intel Xeon 2 3.46 GHz workstation).

The semi-analytical model has been used for all the cases listed in table 1. Figure 2(b) shows the baseline contact stiffness (K_b), which is the contact stiffness when the buried feature is far from the tip. Figure 2(c) shows the contact stiffness variation normalized to the baseline contact stiffness ($\Delta K/K_b$), which is an estimation of the static contrast.

This approach allows for fast evaluation of the behaviors of certain material and load condition combinations. Figure 2(b) shows that the baseline contact stiffness is largely dependent on the size of the scanning tip and the applied force. Figure 2(c) shows that the contrast decreases when using a smaller tip (compare solid triangle cyan and dashed triangle green lines) and decreases further if the depth of the feature is increased (compare solid triangle cyan and solid circle red lines). In all cases an increase in the force results in a contrast increase with the exception of the case of the small tip on a compliant material (purple circle dashed line).

For the latter, the contact pressure is so high that the elastic regime could not be applicable to all load conditions causing a deviation from the behaviour common to all other cases.

The static approach gives a reference for the contact stiffness values reached in the stationary state. However, in current US-AFM techniques, the sample is subjected to an ultrasound wave excitation. The wave excitation is based on modulating a carrier frequency, f_c , with a modulation frequency, f_m , which is equal or close to the contact resonance frequency of the cantilever. Therefore, the acoustic problem must be addressed with a time-dependent approach. The semi-analytical procedure discussed above has been introduced precisely for the purpose of making the dynamic approach feasible in terms of simulation time and available memory. In this section, we refer to case 1 in table 1. The thickness of the silicon layer substrate (h_2) is increased to 550 nm to give more space to the ultrasound waves to propagate before reaching the 2nd layer–1st layer interface. For the cases listed in table 1 the contact radius R_c is less than 10 nm. The contact radius is several orders of magnitude less than the wavelength in the medium at the frequency used ($\lambda \sim 21 \mu\text{m}$ in PMMA at 67 MHz). Any dynamics at the contact volume is negligible with respect to the ultrasound frequency used. This allows to treat the bottom excitation approach with the tip at a fixed position on top of the sample, and a prescribed displacement

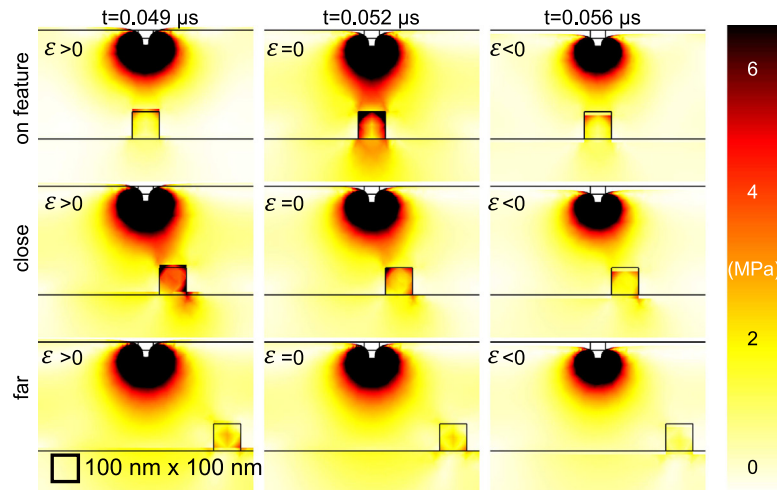


Figure 3. Cross-sectional stress field for different time steps (horizontally) and different positions of the feature with respect to the contact area (vertically). At $0.049 \mu\text{s}$, the substrate is compressed. At $0.052 \mu\text{s}$, the excitation is zero, and at $0.056 \mu\text{s}$, the substrate is under tensile excitation. The non-deformed top surface of the sample and the top layer/substrate and substrate/feature interfaces are marked with black solid lines. The distance between the deformed free-surface and the non-deformed line, ϵ , is indicated as positive when the deformed free-surface exceeds the level of the non-deformed line.

delivered at the bottom surface of the silicon substrate (2nd layer) to simulate an ultrasound plane wave excitation.

An eigenfrequency analysis of the sample has been performed in COMSOL. No external loads are applied, but the sample is constrained on the top surface because of the presence of the tip. The analysis shows that the first eigenmode is a compressional mode at 67 MHz, further (flexural) modes are all above 1 GHz.

In the time-dependent simulations, the prescribed displacement is written as:

$$\delta(t) = \delta_0 \sin(2\pi f_c t) \times \sin(2\pi f_m t) \quad (8)$$

where $\delta_0 = 1 \text{ nm}$, $f_c = 67 \text{ MHz}$ is the carrier frequency and $f_m = [2.20, 2.21, 2.22, 2.23] \text{ MHz}$ is the modulation frequency. In these conditions small differences in the excitation frequency are expected to provide significant differences in the behavior of the system to ultrasound propagation. The modulation frequencies are chosen in the MHz range for simulation time purposes only. In fact, in subsurface US-AFM the modulation frequency is usually selected in the vicinity of the cantilever-sample contact resonance. For a first mode of few hundreds kHz it is interesting to inspect contact frequency shifts of the order of few Hz. However under these conditions the simulation time scale would be exceptionally long before any difference due to modulation is appreciable. Since the aim of the paper is to evaluate the influence of ultrasound modulation on the tip-sample contact stiffness, and not on the cantilever resonance shift, the modulation frequency is chosen in the more convenient MHz range. Each simulations had a total duration of $2.5 \mu\text{s}$ corresponding to more than 100 carrier frequency periods and about 10 modulation frequency periods.

The tip is ensured to be always in contact with the sample, and for simplicity, the nonlinear effects of the tip approaching the sample (for example, Van der Waals forces) are neglected. To ensure this condition throughout the entire simulation time, the tip is pressed on the PMMA layer. Based on the preliminary static simulations, a $0.2 \mu\text{N}$ pre-load gives a static

contact deformation of the PMMA layer of 3.1 nm. This pre-load condition ensures that the $\delta(t)$ displacement excitation never causes a detachment between the tip and the sample.

Since the wavelengths in both the PMMA ($21 \mu\text{m}$) and silicon ($110 \mu\text{m}$) are much larger than the actual medium thickness, there is no signature of wave scattering propagation. The entire medium moves upwards/downwards following the displacement excitation, while the tip is fixed. Figure 3 shows the cross-sectional stress distribution in the case of 2.22 MHz modulation frequency for a few scan steps (vertically) and time steps (horizontally). In all the frames of figure 3, the black solid line at the top of each frame indicates the non-deformed top surface of the sample. At $0.049 \mu\text{s}$, the substrate is compressed: the medium moves upwards, the tip acts as a fixed boundary, the local stress extension at the contact increases and the free surface of the sample exceeds the non-deformed top surface line. At $0.056 \mu\text{s}$, the substrate is under tensile excitation: the medium moves downwards, the local stress extension at the contact is minimum and the free surface of the sample is below the non-deformed line. At $0.052 \mu\text{s}$, the excitation is approximately zero: the free surface of the sample coincides with the non-deformed line. The closer the feature to the tip, the more evident the way in which the stress distribution is distorted by the presence of the feature. The distance between the deformed free-surface and the non-deformed line, ϵ , is the relative displacement between the PMMA surface with respect to the fixed indentation of the tip. From each time frame and for each scan position, the value of ϵ is estimated and is used to calculate the contact stiffness.

Because of the modulated excitation shape, the ultrasound wave has a center frequency at $f_c - f_m$. As a result, the time varying indentation of the tip and the contact stiffness also have the largest spectral component, thus maximum sensitivity, at the frequency $f_c - f_m$. For this reason a pure harmonic centered at the frequency $f_c - f_m$ is used to fit the contact stiffness time trace. The fitted pure harmonic is plotted in figure 4(a) for the modulation frequency of 2.22 MHz for a

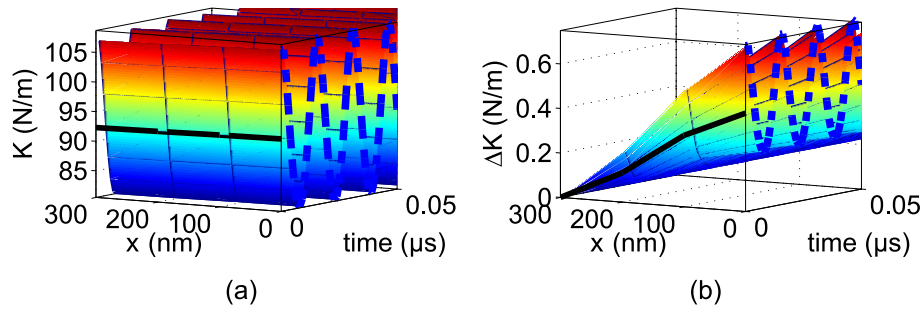


Figure 4. (a) Contact stiffness and (b) variation of contact stiffness at $f_c - f_m$ ($f_m = 2.22$ MHz) as functions of the excitation time and feature scan position. The stationary scan contact stiffness profile is always plotted as a solid black line for reference. The dash-dot blue lines highlight the contact stiffness time profile on-feature.

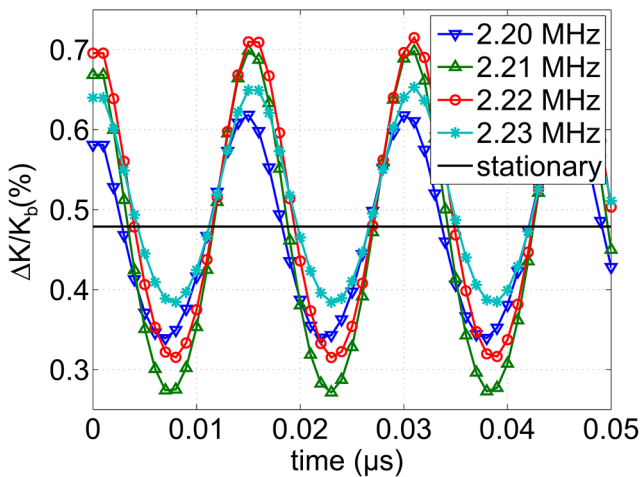


Figure 5. Contact stiffness variation normalized to the baseline contact stiffness ($\Delta K/K_b$) for different modulation frequencies compared to the stationary case.

few periods (time axis), for each scan position of the feature relative to the tip (x -axis).

At each time step, the effects of the ultrasound excitation on the contact stiffness are far larger than the effects of the feature position relative to the tip. For this reason, the off-feature contact stiffness values (at 300nm scan) are subtracted, and the obtained contact stiffness variations are shown in figure 4(b). The comparison with respect to the stationary static case (solid black lines in (a) and (b)) shows that the use of dynamic excitation can induce increased contact stiffness on-feature at the frequency of the maximum energy content $f_c - f_m$.

Furthermore, different modulation frequencies affect the contact stiffness. The low frequency f_m is used to modulate the high frequency f_c thereby obtaining an effective excitation centered at the sum and difference of f_c and f_m . A small change in f_m , thus, results in a small change in the excitation center frequency. Since the kinetic energy is proportional to the square of the frequency, the ultrasound excitation provides a different indentation depending on the center frequency used. In turn the indentation affects the contact stiffness. Figure 5 shows that with modulation frequencies of 2.21 MHz and 2.22 MHz, the normalized contact stiffness variations are higher than for 2.20 MHz and 2.23 MHz.

However with 2.20 MHz and 2.21 MHz the contrast variations are approximately symmetric with respect to the stationary case, while at 2.22 MHz and 2.23 MHz the contrast variations are on average higher than the stationary case. The simulation time is up to $2.5 \mu s$, however the time axis in figure 5 is limited to $0.05 \mu s$.

Therefore, a modulation frequency of 2.22 MHz shows approximately the same contrast as the 2.21 MHz, but it is more efficient since the contrast minima are less pronounced than in the 2.21 MHz case. A non-stationary excitation has effects on the stress distribution at the tip-sample contact. Therefore, the modulation frequency, and thus the slow dynamics of the excitation, can be chosen to maximize the contact stiffness variation and to maximize the average of the time varying contrast with respect to the stationary case. However, the effects of such similar modulation frequencies are also emphasized here because of the choice of the carrier frequency very close to the first eigenfrequency of the system.

In conclusion, we presented 3D ultrasound analysis and simulations of contact stiffness in US-AFM. The local variations in contact stiffness in the volume that is subjected to the ultrasound excitation influences the image contrast in US-AFM. For this reason, the effect of the ultrasound excitation needs to be included in a time-dependent approach. The presented results indicate that a static stationary approach gives an indication of the expected contrast; however, the time-dependent ultrasound approach shows that the choice of the modulation frequency, which is the slow dynamic component in the excitation, allows tailoring and optimization of the contrast.

Acknowledgments

This research was supported by the Netherlands Organization for Applied Scientific Research, TNO, Early Research Program 3D Nanomanufacturing Instruments (www.tno.nl/3dnano/).

References

- [1] Binning G, Quate C and Gerber C 1986 *Phys. Rev. Lett.* **56** 930
- [2] Sadeghian H, Herfst R, Winters J, Crowcombe W, Kramer G, van den Dool T and van Es M H 2015 *Rev. Sci. Instrum.* **86** 113706

- [3] Sadeghian H, Herfst R, Dekker B, Winters J, Bijmagne T and Rijnbeek R 2017 *Rev. Sci. Instrum.* **88** 033703
- [4] Putman C, De Groot B, van Hulst N and Greve J 1992 *J. Appl. Phys.* **72** 6
- [5] Herfst R, Klop W, Eschen M, van den Dool T, Koster N and Sadeghian H 2014 *Measurement* **56** 104
- [6] Turner J and Wiehn J 2001 *Nanotechnology* **12** 322
- [7] Rabe U, Janser K and Arnold W 1998 *Appl. Phys. A* **66** S277
- [8] Parlak Z and Degertekin F L 2013 *Acoustic Scanning Probe Microscopy* ed F Marinello *et al* (Berlin: Springer) ch 15, pp 417–36
- [9] Yamanaka K, Ogiso H and Kolosov O 1994 *Appl. Phys. Lett.* **64** 178
- [10] Rabe U, Amelio S, Kester E, Scherer V, Hirsekorn S and Arnold W 2000 *Ultrasonics* **38** 430
- [11] Striegler A, Koehler B, Bendjus B, Roellig M, Kopycinska-Mueller M and Meyendorf N 2011 *Ultramicroscopy* **111** 1405
- [12] Kimura K, Kobayashi K, Matsushige K and Yamada H 2013 *Ultramicroscopy* **133** 41
- [13] Stan G, King S W and Cook R F 2012 *Nanotechnology* **23** 215703
- [14] Passeri D, Bettucci A and Rossi M 2010 *Anal. Bioanal. Chem.* **396** 2769
- [15] Su C, Tsai T, Liou Y, Lin Z, Lin H and Chao T 2011 *IEEE Electron Device Lett.* **32** 521
- [16] Shi X, Zhang X, Xia T and Fang X 2012 *Nanomedicine* **7** 1625
- [17] Burnham N and Colton R 1989 *J. Vac. Sci. Technol. A* **7** 2906
- [18] Parlak Z and Degertekin F L 2008 *J. Appl. Phys.* **103**
- [19] Hertz H 1896 *Miscellaneous Papers* (London: MacMillan)
- [20] Hanaor D, Gan Y and Einav I 2015 *Int. J. Solids Struct.* **59** 121
- [21] Konter A 2006 *Advanced Finite Element Contact Benchmarks* (Glasgow: National Agency for Finite Element Methods and Standards)